Original Research

Toward Automated Additive Manufacturing of Living Bio-Tubes Using Ring-Shaped Building Units

SLAS Technology
1–13

DOI: 10.1177/2472630320920896
journals.sagepub.com/home/jla
SAGE

Kali L. Manning[1,2], Jacob Feder[1], Marianne Kanellias[1,2], John Murphy III[1], and Jeffrey R. Morgan[1,2]

Abstract

Tissue engineering has been largely confined to academic research institutions with limited success in commercial settings. To help address this issue, more work is needed to develop new automated manufacturing processes for tissue-related technologies. In this article, we describe the automation of the funnel-guide, an additive manufacturing method that uses living tissue rings as building units to form bio-tubes. We developed a method based on 96-well plates and a modified off-the-shelf liquid-handling robot to retrieve, perform real-time quality control, and transfer tissue rings to the funnel-guide. Cells seeded into 96-well plates containing specially designed agarose micromolds self-assembled and formed ring-shaped microtissues that could be retrieved using a liquid-handling robot. We characterized the effects of time, cell type, and mold geometry on the morphology of the ring-shaped microtissues to inform optimal use of the building parts. We programmed and modified an off-the-shelf liquid-handling robot to retrieve ring-shaped microtissues from the 96-well plates, and we fabricated a custom illuminated pipette to visualize each ring-shaped microtissue prior to deposit in the funnel guide. Imaging at the liquid-air interface presented challenges that were overcome by controlling lighting conditions and liquid curvature. Based on these images, we incorporated into our workflow a real-time quality control step based on visual inspection and morphological criteria to assess each ring prior to use. We used this system to fabricate bio-tubes of endothelial cells with luminal alignment.

Keywords

microtissue manipulation, biofabrication, additive manufacturing, automation, quality control

Introduction

Living tissue-engineered products have the potential to serve as platforms for drug discovery and toxicity testing as well as implants to replace damaged or diseased tissues and organs grafts. However, successful commercialization of tissue-engineered products has been limited because of a number of factors, including challenges in manufacturing. Most tissue-engineered products are fabricated one at a time using labor-intensive methods. As outlined by the Advanced Regenerative Manufacturing Institute, automation and monitoring (quality control; QC) of tissue production are essential to commercial translation.[1] Automation can decrease cost and increase throughput and output while decreasing human error and increasing product fidelity due to the addition of QC metrics. Although automation methods exist for the culture of cells in two dimensions, there has been limited development in the automation and scale up of three-dimensional (3D) tissue-engineered products.[2]

Bio-printing is a common additive manufacturing approach to fabricating tissue-engineered products. Three-dimensional macro-structures such as valves and tubes have been built drop by drop using liquid polymer scaffolds containing cells.[3–9] However, bio-printing has several limitations yet to be overcome. The density of cells in the polymer scaffold is low and does not equal that of most tissues and

[1]Department of Molecular Pharmacology, Physiology and Biotechnology, Brown University, Providence, RI, USA
[2]Center for Biomedical Engineering, Brown University, Providence, RI, USA

Received Jan 17, 2020, and in revised form Mar 19, 2020. Accepted for publication Mar 26, 2020.

Supplemental material is available online with this article.

Corresponding Author:
Jeffrey R. Morgan, Brown University, G-B 393, Biomed Center, 171 Meeting St., Providence, RI 02912, USA.
Email: Jeffrey_Morgan@Brown.edu

organs. Polymerization of the scaffold occurs in air, and so the ultimate size of the printed construct is limited because cells cannot be maintained in the liquid nutrient culture medium they absolutely require.[10] Lastly, bio-printing requires the delivery of tens of thousands of small drops (manufacturing steps), and strategies to control the quality of those steps have yet to be developed.

An alternative additive manufacturing approach is the manipulation and placement of 3D microtissue building units composed of cells that have aggregated and self-assembled. These microtissues are formed without the use of a scaffold, have a high cell density comparable with normal tissue and organs, and will fuse with one another while submerged under cell culture medium.[11–15] Microtissue building units are easily fabricated using hanging drop or micromolding techniques and have been formed in a variety of shapes including spheroids, rods, rings, and honeycombs, with cell numbers ranging from as few as about 500 cells per spheroid to more than 11 million cells per honeycomb. Moreover, as discrete building units of hundreds to thousands of cells, they significantly decrease the number of building steps and lend themselves to new strategies and metrics for QC.[16–18]

Currently available methods to manipulate microtissues include the Kenzan method; the Bio-Pick, Place and Perfuse (Bio-P3); and the Funnel-Guide. The Kenzan method uses a robotic arm to aspirate up and then precisely pierce spheroids onto a microneedle array where they fuse with one another.[19–22] The Bio-P3 uses fluid suction through a membrane to grip and move honeycomb building parts through culture medium and stack them onto a build head, where the microtissue layers fuse and their lumens are perfused with culture medium during the build.[23–25] The funnel-guide uses a funnel-shaped vessel to stack ring-shaped microtissues that have been added one at a time using a standard liquid-handling pipette. As the ring-shaped microtissues fall through the culture medium, the funnel-guide guides them to form a stack of living rings that fuse into a single bio-tube.[26] Major advantages of the funnel-guide are cost and simplicity of use and design. Living building parts are not gripped, nor are they pierced; they are retrieved with a pipette. Moreover, minimal accuracy and precision are required to deliver rings to the large mouth of the funnel-guide. Unlike mechanized approaches that can be limited by the accuracy, precision, and expense of their motors, the accuracy and precision of the inexpensive funnel-guide is dictated by the dimensions of its stem.

In this study, we have automated the workflow of the funnel-guide. We scaled up the production of ring-shaped tissues by using 96-well plates and modified a liquid-handling robot to retrieve the rings, one at a time, and deliver them to the funnel-guide. Prior to delivery, each ring passes a real-time QC step based on images obtained from an upward facing camera. The resulting automated workflow uses rings to build living bio-tubes layer by layer, is applicable to multiple cell types, and is an advancement toward the manufacture of 3D tissue-engineered products.

Materials and Methods

Cell Culture, Micromold Fabrication, and Formation of Ring-Shaped Microtissues

Human hepatocellular carcinoma (HepG2) cells were expanded in Eagle's Minimum Essential Medium (EMEM; Corning Incorporated, Corning, NY) supplemented with 10% fetal bovine serum (Thermo Fisher Scientific, Waltham, MA) and 1% penicillin/streptomycin (MP Biomedicals, LLC, Santa Ana, CA). Human umbilical vein endothelial cells (HUVECs) were expanded in endothelial growth medium (EGM) with Supplement Kit (PromoCell, Heidelberg, Germany) and 1% penicillin/streptomycin (MP Biomedicals, LLC). Cultures were maintained in a 37 °C, 5% CO_2 atmosphere. Cells were trypsinized, counted, and resuspended to the desired cell density for each experiment.

Agarose gels were cast from 3D Petri Dish micromolds (Microtissues, Inc., Providence, RI) as previously described.[24] Ninety-six-well agarose gels were cast from either PEEK or stainless-steel molds (Proto Labs Inc., Maple Plains, MN). Briefly, 90 µL (PEEK mold) or 80 µL (stainless-steel mold) of molten agarose was pipetted into the 96-well plate, and a drop of agarose was placed into the recesses in the mold before inverting and placing into the 96-well plate. Once the agarose solidified, the mold was removed. Gels were equilibrated in serum-free EMEM or EGM at 37 °C and 5% CO_2 for 24 h prior to use. Agarose gels were made with powdered agarose (low electroendosmosis/multipurpose/molecular biology grade; Fisher BioReagents, Thermo Fisher Scientific, Waltham, MA), sterilized by autoclaving, and then dissolved in sterile water to 2% (weight/volume). 3D Petri Dish recesses were 1400 µm in diameter with a central agarose peg of 600 µm and surrounding 400 µm trough and contained 36 recesses per gel. Ninety-six-well recesses were 2200 µm in diameter with a central agarose peg of 1400 µm and a surrounding 400 µm trough. Each well contained an agarose gel with a single ring-shaped recess. Gels were seeded at a density of 50,000, 75,000, or 100,000 cells per feature or 100,000, 150,000, or 200,000 cells per 96-well feature. Cells aggregated in the micromolds and self-assembled microtissues were used 4 h after cell seeding.

Evaluation of the Morphological Changes of Tissue Rings

Tissue rings were either imaged inside agarose molds or transferred using a wide-bore pipette tip into 96-well plates with agarose-coated wells equilibrated with culture medium.

Snapshot and time-lapse imaging was performed using a Zeiss Axio Observer Z1 equipped with an AxioCam MRm camera with ZEN software (Carl Zeiss Microscopy, LLC, Thornwood, NY). Side-view imaging was performed by transferring rings into a cuvette (Dynalon Corporation, Rochester, NY) filled with growth medium. Images were captured using a DinoLite digital microscope (BigC DinoLite, Torrance, CA). Tissue ring release from the micromold was quantified in a Kaplan-Meier curve, in which release from the mold was an event. Tissue formation only counted rings with the potential to form; mold defects were excluded from analysis. Measurements of cross-sectional area (A_C) were obtained using a thresholding macro on ImageJ (National Institutes of Health, Bethesda, MD). Measurements of the ring outer diameter (D_O) and lumen diameter (D_L) were obtained using Zen software by taking the average of the vertical and horizontal measurement of each parameter. Thickness ($T_{x,y}$) of the rings in the *x,y* dimensions was calculated by

$$D_O - D_L / 2. \quad (1)$$

Measurements of A_C, D_O, D_L, and $T_{x,y}$ were normalized to the T = 0 measurements. Height (H) measurements were taken using ImageJ (National Institutes of Health). Ring volume was calculated by

$$V = (\pi hr)(2\pi R) \quad (2)$$

where *h* is the semi-minor axis of the ellipsoid cross section ($H/2$, where *H* is the total measured height of the ring), *r* is the semi-major axis (or radius, calculated as $T/2$), and *R* is the major radius of the top-down shape, calculated as

$$(r + (D_L / 2)). \quad (3)$$

Fabrication and Use of the Funnel Guide

Funnel-guide negative replicas were fabricated as previously described.[26] Briefly, SolidWorks (Dassault Systems SolidWorks Corporation, Waltham, MA) was used to design the negative, which consisted of three chambers: a free-fall chamber, a funnel-chamber, and a stacking chamber. Free-fall and funnel-chamber dimensions remained the same at 8 mm × 8 mm and 10 mm in height, and 77° and 13 mm in height. The stacking-chamber dimensions were 1.9 mm in diameter and 10 mm in height, to accommodate the 96-well rings. The negative replicas of the funnel-guide were 3D printed by Proto Labs. Funnel-guides were then fabricated by pouring polydimethylsiloxane (PDMS) (SYLGARD 184 Silicone Elastomer Kit, Dow Chemical Company, Midland, MI) into a cuvette (Dynalon Corporation, Rochester, NY). PDMS was cured for 1 h at 100 °C and then overnight at room temperature. The funnel-guide negative replica was removed, leaving behind a void in the PDMS in the shape of the desired funnel-guide. The inside was then coated with a 3% (weight/volume) Pluronic F-68 (Sigma-Aldrich, St. Louis, MO) solution overnight.

Automated Fabrication of Bio-Tubes

To automate the fabrication of bio-tubes using the funnel-guide, an OpenTrons OT-One (Brooklyn, NY) was modified accordingly. The A-axis motor and drive assembly were unplugged and removed. The pipette was relocated to be driven by the B-axis, which was plugged into the A-axis. The *z*-axis was extended vertically by adding a piece of aluminum stock frame (McMaster Carr, Elmhurst, IL). The A-axis limit switch was repurposed to be the *z*-axis probe limit switch and was connected to the B-axis limit switch input, which was reconfigured to act as the probe. To probe the *z* height, the limit switch and spring steel flexures (McMaster Carr, Elmhurst, IL) were mounted on a custom pipette tip holder designed using SolidWorks (Dassault Systems SolidWorks Corporation, Waltham, MA) and 3D printed using Shapeways 3D Printing Company services (Shapeways HQ, New York, NY).

A LabVIEW (National Instruments, Austin, TX) interface was created to control the OpenTrons OT-One liquid-handling robot. At startup, the user calibrates the positions of the pipette tip, well A1 of the 96-well plates, the camera, and the funnel-guides. The user can input the number of 96-well plates and funnel-guides to be used. Located at the bottom of the LabVIEW interface is the Advanced Parameter Area, which contains the parameters that affect ring pickup from the 96-well plate. These parameters include "well height," the height above the bottom of the well from which the robot pipettes; "federate," the rate of aspirating and dispensing; "disp," the baseline position for the pipette/A axis; "asp," the distance the robot moves the pipette plunger up and down to aspirate and dispense; "extra liquid," the additional aspiration distance to allow for reverse pipetting; "meniscus comp," the distance to move the pipette plunger down before taking a picture for QC in order to change the curvature of the meniscus; "agitation count," the number of times to pipette while in the well; and "speed," the rate the pipette moves along its axes. Once calibrated and all parameters set, the user presses "Build," which initiates the following sequence: move to pipette tip rack, move to well A1, probe *z* height until limit switch activated, move to well B1, pick up tissue ring, move to camera, perform QC, place tissue ring in funnel-guide or back in 96-well plate depending on the outcome of QC, move to well C1, repeat loop until all 96-well plates have been used, return home. Throughout the build process, parameters can be changed in real time by the user if needed.

Real-Time QC of Ring-Shaped Tissue-Building Parts

A camera (Blackfly S model; FLIR Systems, Inc., Wilsonville, OR) and lens (2×, 0.10 NA; Ultra Compact Objective, Edmund Optics Inc., Barrington, NJ) were mounted in an upward-facing orientation to the base of the OT-One. Our custom pipette tip holder was designed to hold a black pipette tip (TipOne for Tecan Genesis and Freedom EVO; Tecan, Männedorf, Switzerland), 1/8 inch diameter acrylic light pipe (McMaster Carr, Elmhurst, IL), and a custom printed circuit board (PCB) assembly containing a light-emitting diode (LED) and constant-current driver electronics (JLCPCB, Shenzhen, Guangdong, China) to back light the ring-shaped tissue while inside the pipette tip. During the build process, a single image of the ring in the pipette tip was taken. This image was used by our custom QC algorithm to perform real-time analysis of ring metrics. The QC algorithm uses the LabVIEW (National Instruments) "Find Circular Edges 3 VI" to identify the tissue ring. Briefly, the algorithm finds a circular edge according to the input parameters within a given region of interest (ROI). The search area is the area between two concentric rings; the algorithm generates lines between the inner and outer ring and then calculates the gradient of the image along those lines. For each line, the spot with the largest gradient becomes a hit point, which is then used to create a circle of best fit, the output of the algorithm. This analysis was conducted three times: first using the entire image as the ROI to identify the pipette tip, then using the area of the pipette tip as the ROI to locate the outer edge of the tissue ring, and finally using the outer edge as the ROI to identify the lumen of the tissue ring.

QC values were set through analysis of five plates of HUVEC 150K 4h tissue rings. QC measurements were taken using an offline LabVIEW VI, averaged, and the range set to two standard deviations from the mean. For inner and outer diameter measurements, QC LabVIEW values were converted to metric units by fitting a linear trend to a data set of QC values and measured diameter values taken in ZEN software. The determined equation was

$$y = 2.7351x - 76.485 \quad (4)$$

where y represents the measured value and x represents the QC value from LabVIEW.

Evaluation of Automated Funnel-Guided Fabrication

The modified OT-One system was used to build a bio-tube composed of 30 vertically aligned HUVEC 150K 4h tissue rings. Six bio-tubes were fabricated, and success was determined through visual inspection as each tissue ring was placed into the funnel-guide. Images of the bio-tube were taken using a Pixel 3 camera (Alphabet Inc., Mountain View, CA) throughout the building process, at 5 rings high, 15 rings high, and 30 rings high. To evaluate the alignment of the tissue rings, a top-view image was taken using an Olympus SZ-PT dissecting microscope (Olympus Corporation, Shinjuku, Japan) and Pixel camera (Alphabet Inc.).

Statistical Analysis

Statistical analysis was conducted on JMP software (SAS Institute Inc., Cary, NC). The significance for A_C, D_O, D_L, and $T_{x,y}$ was determined using a multivariate analysis of variance (MANOVA) with full factorial analysis for the repeated measurement of time, in which significance denotes $p < 0.05$. Data analyzed by MANOVA were first examined using a Shapiro-Wilk test to determine that the data came from a normal distribution. A_C data were Log_{10} transformed to achieve normality. Ring formation as a function of peg angle and cell type was analyzed using a logistic regression in which significance denotes $p < 0.05$. Data were first examined using Shapiro-Wilk test to determine that the data came from a normal distribution. The significance between Kaplan-Meier survival curves was tested via pairwise Log-rank analysis ($p < 0.05$) with Cox's proportional hazard regression analysis used for multivariable comparison ($p < 0.005$).

Results

Tissue Rings Undergo Morphological Changes

To determine the morphological changes that occur when tissue rings are self-assembled, we seeded HUVECs in agarose micromolds containing 36 ring-shaped features composed of a circular trough (400 μm wide, 1400 μm outer diameter) surrounding a central agarose peg (600 μm diameter). Cells were seeded at 5×10^4, 7.5×10^4, or 1×10^5 cells per ring, and brightfield images were obtained every 30 min for 20 h (**Fig. 1**). Within hours, the cells self-assembled a ring-shaped tissue that contracted around the central agarose peg. Over time, these HUVEC rings moved up the agarose peg and released themselves from the micromold (**Suppl. Video 1**). The percentage of tissue rings in the mold that had not yet released themselves (survival) was plotted as a function of time as a Kaplan-Meier survival curve for each cell-seeding density and compared. The survival of tissue rings seeded with the lowest cell number (5×10^4 cells/ring) was significantly longer at 13 h of median survival time (determined by parametric model analysis with Weibull probability fit) than the higher cell-seeding numbers. This group also showed less variation in the rate of loss (standard deviation from mean) than the higher seeding numbers.

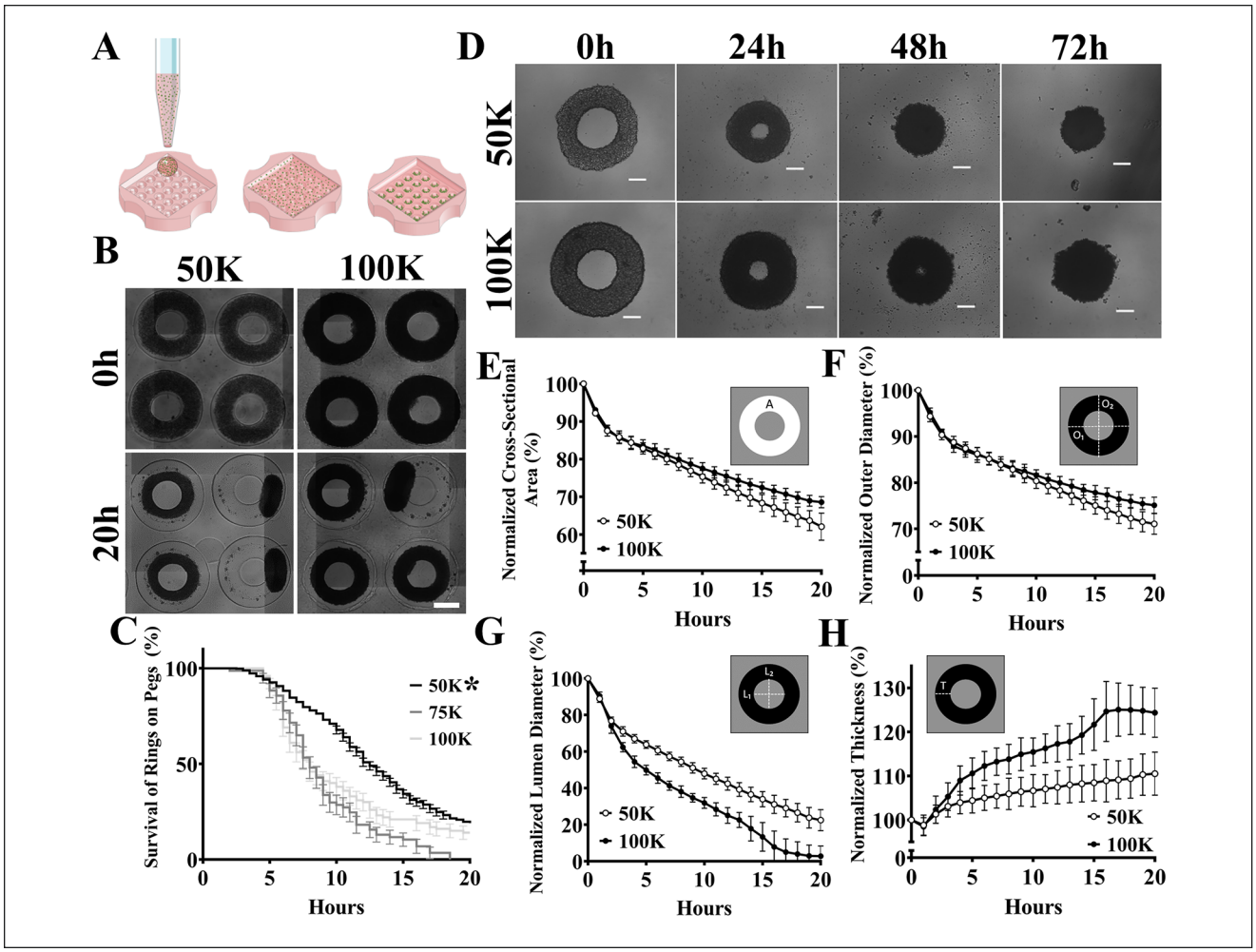

Figure 1. Tissue rings undergo morphological changes. Schematic of the process to form self-assembled tissue rings (**A**). Rings of human umbilical vein endothelial cells (HUVECs) were formed by seeding cells into an agarose mold, where cells settled into ring-shaped recesses and self-assembled. Rings (5×10^4 cells/ring and 1×10^5 cells/ring) were imaged inside the mold at 0 h and 20 h using brightfield microscopy (**B**). Scale bar is 200 µm. Rings that moved up and off the agarose peg were plotted as a survival curve for three seeding numbers, 5×10^4, 7.5×10^4, and 1×10^5 cells/ring, with * denoting statistical significance of $p < 0.05$ ($n = 534$, 78, 108, respectively) (**C**). HUVEC rings (50K and 100K) were removed from the mold at 6 h, placed on an agarose surface, and imaged over 72 h (**D**). Scale bars are 200 µm. Released HUVEC rings were imaged every 30 min for 20 h, and the following parameters measured and normalized to $T = 0$ measurements: cross-sectional area (**E**), outer diameter (**F**), lumen diameter (**G**), and thickness *x, y* (**H**). There was a significant change in all parameters over time, and seeding density affected these changes. Where 50K decreased more in A_c and D_O, 100K decreased more in D_L, and 100K increased more in T_{xy} ($n = 27$ for 50K and $n = 15$ for 100K). Measurements for A_C were Log_{10} transformed for statistical analysis, with significance calculated by multivariate analysis of variance, $p < 0.05$.

To determine the morphological changes of rings outside of the mold, HUVEC rings formed from 5×10^4 and 1×10^5 cells per ring were removed from the molds after 6 h of self-assembly, placed in a 96-well plate coated with agarose, and imaged over 3 d. By 72 h, the rings contracted and closed their lumens. To quantify the rate of these morphological changes, we imaged rings every 30 min for the first 20 h. From these images, we measured the cross-sectional area of the ring (A_c), outer diameter of the ring (D_O), diameter of the ring's lumen (D_L), and width of the ring measured in the *x, y* dimensions (T_{xy}). All values were normalized to the starting value and plotted over time. Cross-sectional area, outer diameter, and lumen diameter significantly declined over 20 h, and this decrease was significantly affected by seeding density, where 5×10^4 cells per ring had a greater rate of decrease over time than 1×10^5 cells per ring. Ring thickness significantly increased over time, with 1×10^5 rings increasing significantly more than 5×10^4 rings. There was a significant difference between seeding density and time on ring thickness, where the seeding density significantly affected the rate of change. To examine these changes more closely, we measured

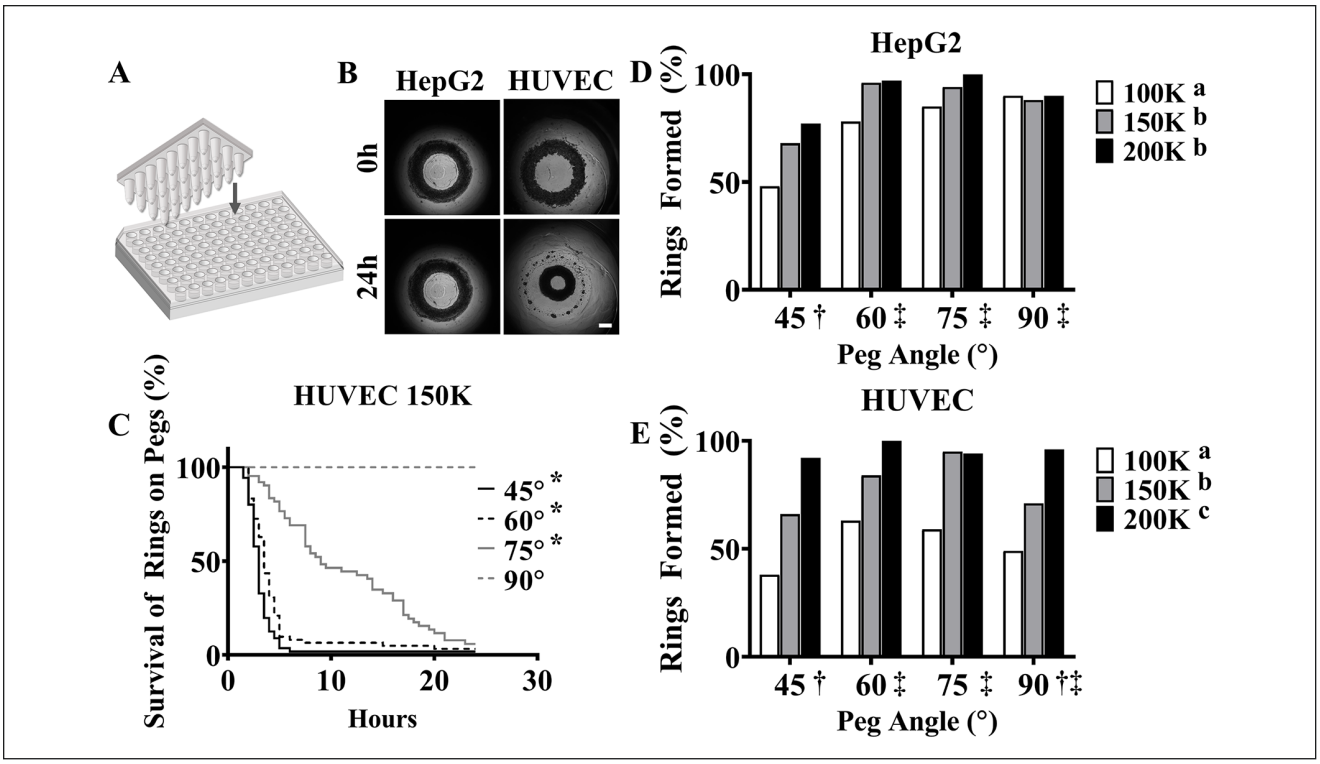

Figure 2. Tissue rings produced in a 96-well plate. Schematic of mold used to form one ring-shaped recess per well (**A**). Plates were fabricated by pipetting molten agarose into the plate, inserting the mold, and removing the mold after the agarose gelled. The tissue ring surrounds a central peg of agarose, and four angles of this peg were tested: 45°, 60°, 75°, and 90°. Rings (1.5×10^5 cells) formed on 60° pegs using HepG2s and human umbilical vein endothelial cells (HUVECs), imaged at 0 h and 24 h (**B**). Scale bar is 500 μm. HUVEC rings (150K) self-released from the mold are plotted as a survival curve as a function of peg angle, with * denoting statistical significance at $p < 0.05$ ($n = 219$) (**C**). Ring formation plotted as a function of peg angle for three seeding densities and two cell types, HepG2 (**D**) and HUVEC (**E**). For HepG2 rings, 60°, 75°, and 90° formed significantly more rings than 45°, and 100K formed significantly fewer rings, with peg angle having the greatest impact. For HUVEC rings, 60° formed significantly more than 45°, and 75° formed significantly more than 45°. 150K cells formed significantly more than 100K, and 200K formed significantly more than 150K and 100K ($n = 239$, 253, and 254 for HepG2 100K, 150K, and 200K, respectively; $n = 213$, 219, and 228 for HUVEC 100K, 150K, and 200K, respectively).

height (z) from side-view images (1×10^5 and 5×10^4 cells/ring) and compared that to width (x, y) at time 0 and 20 h (**Suppl. Fig. S1**). Increased cell number increased the width as well as the height. For both cell numbers, width and height increased with time, but this effect was significant only for the highest cell number. These measurements allowed us to calculate the volume of the rings as a function of time. For both cell numbers, volume declined with time, and the greater decrease occurred with the lower cell number (30% ± 3.6% vs 19% ± 3.9%). Ring volume decreased with time despite the increase in thickness and height, because the ring's outer diameter decreased significantly over time. The volume decrease was likely due to increased packing of cells and/or the decrease in cell volume.

Production of Tissue Rings in a 96-Well Plate

To adapt the agarose molds to an automated workflow, we designed a new molding system for 96-well plates so that each well has one circular feature molded in agarose that, when seeded with cells, forms one ring-shaped tissue per well (**Fig. 2**). To form these 96-well plates, molten agarose was added to each well, and a mold was inserted into the plate. After the agarose gelled, the mold was removed. To facilitate the easy retrieval of tissue rings from the wells, we altered the angle of the central agarose peg and tested angles of 45°, 60°, 75°, and 90° (**Suppl. Fig. S2**). All four angles were successfully molded in a 96-well plate, forming circular troughs that were 2200 μm in diameter with a central peg 1400 μm in diameter and a surrounding 400 μm trough.

To test these angles, we seeded plates with HUVEC or HepG2 cells at 1.0, 1.5, or 2.0×10^5 cells per well. Time-lapse videos showed that HUVECs (1.5×10^5) formed rings that moved up and off the 60° peg by 24 h (**Suppl. Video 2**). In contrast, HepG2 cells formed rings that stayed on the 60° peg at 24 h. To evaluate ring formation, we measured the number of intact rings at 24 h and plotted this as a function of peg angle for both cell types at three seeding

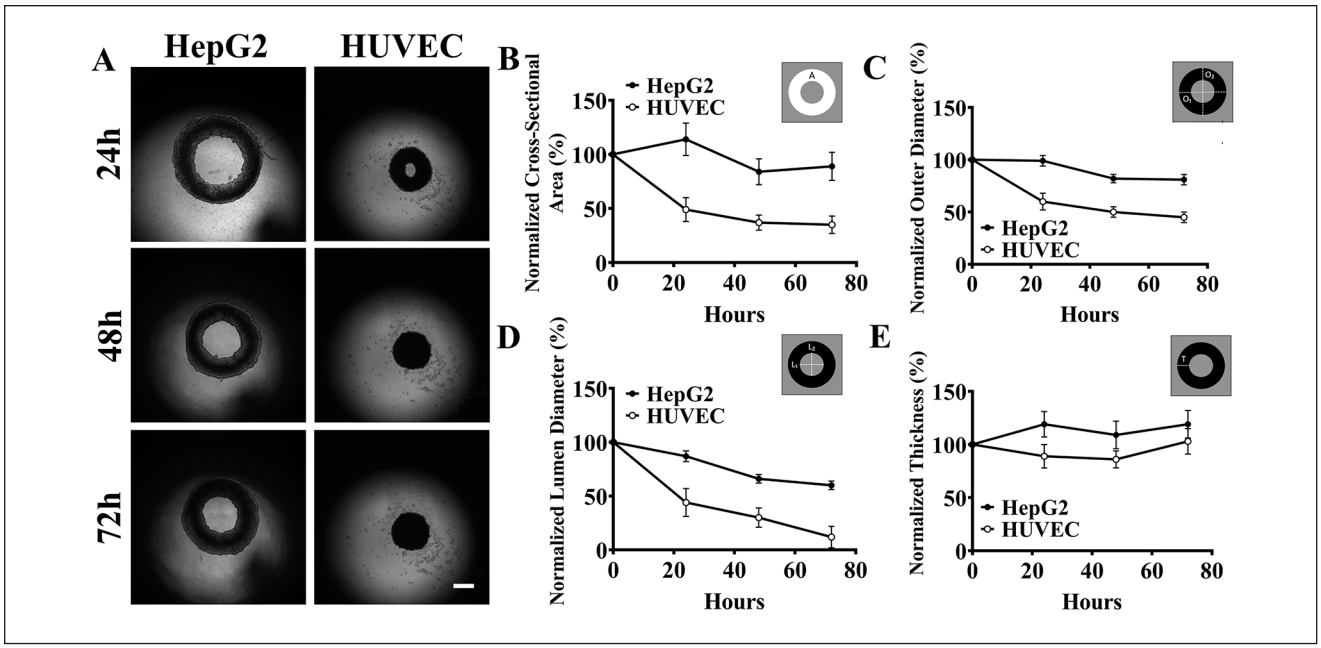

Figure 3. Morphological changes of tissue rings are cell type dependent. Rings were formed by seeding 1.5 × 10^5 HepG2 cells and human umbilical vein endothelial cells (HUVECs) into 96-well plates with agarose recesses each with a 60° peg, grown for 24 h, removed, and placed on a nonadherent agarose surface. Images were acquired at 24 h, 48 h, and 72 h using brightfield microscopy (**A**). Scale bar is 500 µm. Ring cross-sectional area (**B**), outer diameter (**C**), lumen diameter (**D**), and thickness (**E**), plotted as a function of time. All four parameters changed significantly over time, with the rate of change being affected by cell type and where HUVEC rings changed significantly more than HepG2 rings did (n = 23 and 36 for HepG2 and HUVEC, respectively). Significance calculated by multivariate analysis of variance, $p < 0.05$.

densities. The highest percentage of rings formed in wells with 60° and 75° pegs with seeding densities of 1.5 × 10^5 and 2.0 × 10^5. HepG2 ring formation was affected the most by peg angle, where 60°, 75°, and 90° pegs formed significantly more rings than 45° pegs. In contrast, HUVEC ring formation was affected the most by seeding density, where 1.0 × 10^5 cells formed significantly fewer rings. The 60° and 75° pegs formed significantly more HUVEC rings than the 45° pegs. We determined 45° to have a significantly shorter survival time than 60° and 75° pegs at 3 h, 60° to have a significantly shorter survival time than 75° and a significantly longer survival time than 45° pegs at 4 h, and 75° to have a significantly longer survival time than both 60° and 45° pegs at 10 h. Based on these data, we elected to use HUVEC rings formed from 1.5 × 10^5 cells on a 60° peg and harvested at 4 h to test our automated work flow. Rings formed on 90° pegs were more stable but could not be reliably removed from the peg with a pipette.

To determine the morphological changes of HepG2 and HUVEC rings formed using 96-well plates, tissue rings (1.5 × 10^5 cells) were removed from the molds after 24 h of self-assembly and placed in a 96-well coated with agarose (**Fig. 3**). Rings were imaged every 24 h, and parameters of cross-sectional area (A_c), outer diameter (D_O), lumen diameter (D_L), and thickness (T_{xy}) were measured, normalized to the starting value, and plotted over time. As expected, there was a decrease in A_c, D_O, and D_L for HUVEC rings. This decrease was significant, with HUVEC rings decreasing significantly more than HepG2 rings over time. Thickness also changed significantly over time, with a statistically significant difference between HUVEC and HepG2 rings. Cell type significantly affected the rate of change for all four variables.

Automated Workflow for Tissue Rings

To determine if tissue rings could be retrieved from the 96-well plates and delivered one at a time to the funnel-guide for biofabrication, we created a custom LabVIEW interface to control a liquid-handling robot as it executed an automated workflow (**Fig. 4**; **Suppl. Fig. S3**). The main components of the repetitive workflow are as follows: (1) liquid suction via a pipette to retrieve one tissue ring from one well of a 96-well plate, (2) movement of pipette-containing tissue ring to a location directly over an upward-facing camera to image the tissue ring, (3) image-based QC of the tissue ring, and (4) delivery of the tissue ring to the funnel-guide, or back into the 96-well plate depending on the QC outcome. To ensure retrieval of the tissue rings, the tip of the pipette was moved to a specified and precise height within each well of the 96-well plate. To remove variability in tip height in each 96-well plate, we designed a

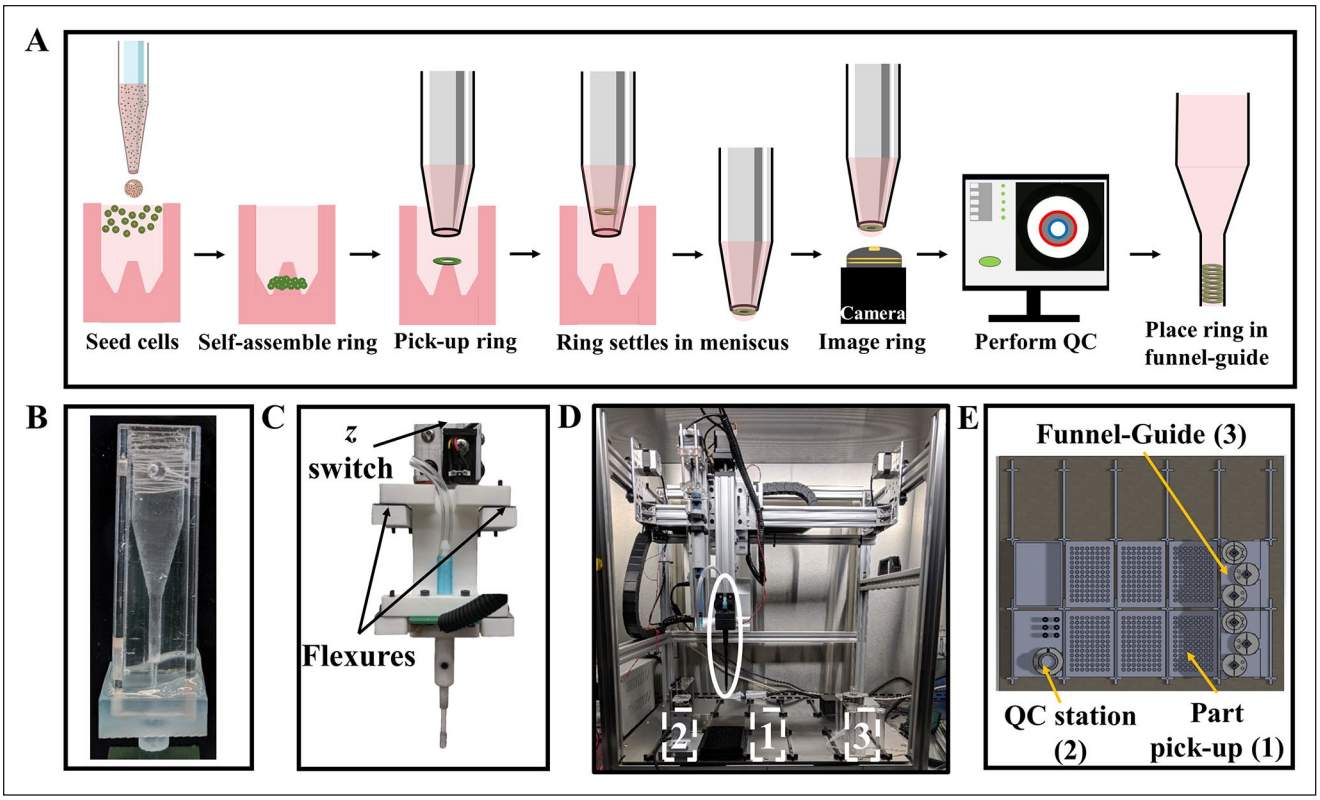

Figure 4. Automated workflow to use tissue rings in biofabrication. Schematic of the key steps in the workflow of a liquid-handling robot (**A**). Tissue rings were fabricated by seeding cells into a 96-well plate. Tissue rings self-assemble, one per well. A liquid-handling robot uses a pipette to retrieve a ring. The ring in the pipette settles to the tip's bottom, and the pipette is moved over an upward-facing camera to image the ring. The image is used to perform quality control using a custom algorithm. Depending on the outcome of the image-based quality control algorithm, rings are placed either in a funnel-guide (3) (**B**) or put back in the 96-well plate. A custom pipette tip holder with mounted flexures and z-limit switch ensures the pipette tip goes to the same height in each well (**C**) (circled in [**D**]). Snapshot and schematic of the Opentrons OT-1 liquid-handling robot with areas designated for part pickup (1), image-based quality control (2), and funnel-guide building area (3) (**D**, **E**). The steps of the build workflow run on a loop until all ring building parts have been used.

custom pipette tip holder with a mounted flexure and *z*-limit switch, which was triggered by probing the depth of the first well of the 96-well plate with the pipette tip at start up (**Suppl. Video 3**). To evaluate the retrieval of tissue rings, we imaged 96-well plates prior to ring retrieval and cross-referenced with QC images to calculate the percentage success of ring retrieval. The 4h 150K HUVEC rings had a pick-up percentage of approximately 88%.

To acquire the QC images of the tissue rings while in the pipette, we designed a custom pipette holder and optimized the lighting conditions (**Fig. 5**). Within seconds of being retrieved from a well, a tissue ring settles by gravity to the bottom of the liquid being held by the pipette tip. The ring, which is horizontal and parallel to the air-liquid interface, can be imaged by an upward-facing camera, but we found that lighting was critical for obtaining images suitable for real-time QC. We tested ambient light, side light, back light, and combinations of the three and determined that back lighting via an LED coupled to an acrylic light pipe in the pipette provided reproducible images with a white background and the sharpest contrast between the tissue ring and the pipette tip. We also eliminated the interfering effects of ambient light by using a black pipette tip. In addition to light intensity, we also found that the curvature of the liquid upon which the tissue ring was resting was another factor influencing image quality. Slight downward adjustments of the pipette's plunger that increased the liquid's curvature could also significantly improve image quality. To address this issue, we created in the LabVIEW interface a liquid curvature compensation parameter that can be adjusted to alter the liquid's curvature in real time. Using our custom imaging setup, we imaged more than 900 HUVEC rings (1.5×10^5 cells) and obtained an imaging success rate of 94%.

Tissue Rings Can Be Quality Controlled in Real Time

To determine if rings could be located and analyzed while inside the pipette tip, we developed a LabVIEW algorithm

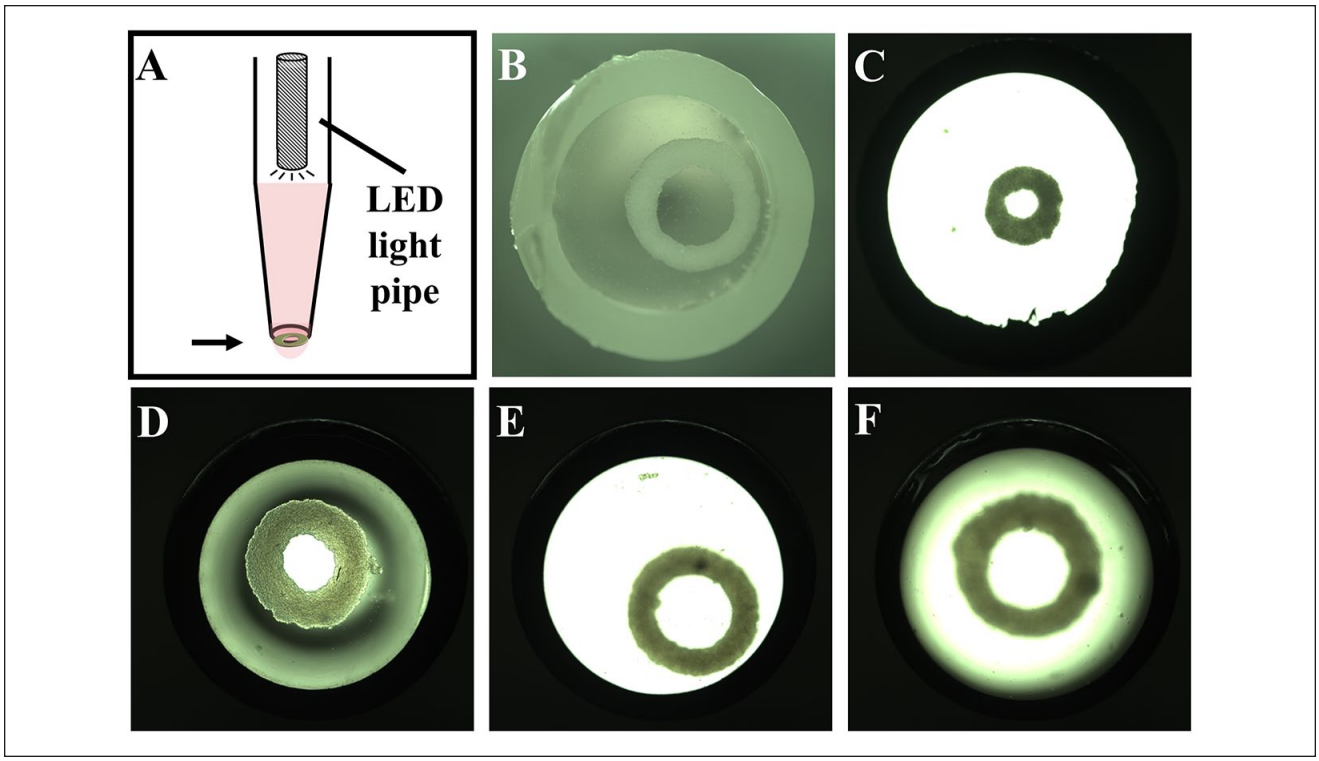

Figure 5. Imaging of retrieved tissue rings. Schematic of a custom-designed pipette tip holder built to house the pipette tip and the back-lighting system to take images of a tissue ring when it is positioned over the upward-facing camera. The light source is a light-emitting diode mounted to a PCB, with a potentiometer to control intensity. The light is directed to the tissue ring via a light pipe inserted into the pipette tip (**A**). The method of lighting influences image quality. Image of a tissue ring in a conventional translucent tip with ambient light (**B**). Image of a tissue ring in a black opaque tip with back lighting (**C**). Curvature of the liquid at the end of tip influences image quality. Stepwise adjustments of the pipette's plunger that progressively increase the liquid's curvature also alter the quality of the image (**D–F**).

to process and analyze the images (**Fig. 6**). The algorithm identifies the tissue ring by finding circular edges via a search within a given ROI and the identification of the largest gradient between two concentric rings. First, the algorithm uses the entire image as its ROI to identify the inner edge of the pipette tip. After this inner edge is located, the algorithm uses this new area as the ROI to identify the outer edge of the tissue ring. Finally, it uses the outer edge of the tissue ring as the ROI to identify the inner edge, or the lumen, of the tissue ring. Once the tissue ring has been identified, it can be evaluated using parameters of center distance, inner diameter, inner roundness, outer diameter, and outer roundness (**Suppl. Fig. S4**). To determine the parameter range for HUVEC rings (1.5×10^5 cells), we retrieved tissue rings from five 96-well plates, imaged the rings, and measured these parameters. Parameters were determined for center distance (108), inner diameter (199–353), inner roundness (0.001–16), outer diameter (603–722), and outer roundness (0.001–30). QC values for the inner diameter and outer diameter correspond to lumen diameters of 469 to 890 µm and outer diameters of 1578 to 1900 µm. Our test of the algorithm showed that it was able to perform its measurements successfully on 71% of the imaging events of HUVEC rings. The proportion of events (29%) that were unsuccessful were due to the inability of the algorithm to perform any one of its five measurements (center distance, inner diameter, inner roundness, outer diameter, and outer roundness.

Bio-Tube Fabrication Can Be Automated

To determine if we could automate the funnel-guided fabrication of bio-tubes, we used the developed liquid-handling workflow with real-time QC to fabricate six bio-tubes, with each containing 30 tissue rings (**Fig. 7**). The bio-tubes were fabricated with tissue rings that were successfully picked up, imaged, and passed the QC step. As each ring was placed in the funnel-guide, it self-righted to a horizontal orientation, was guided down to the stacking chamber, and settled to create an aligned stack of tissue rings (**Suppl. Video 4**). The maximum number of rings that can be stacked is dictated by the length of the stacking chamber and the height of each ring. HUVEC rings have a height of about 275 µm, and the length of the stacking chamber we tested was 10 mm, so it can accommodate about 36 rings. Longer stacking chambers can easily be fabricated if needed. To

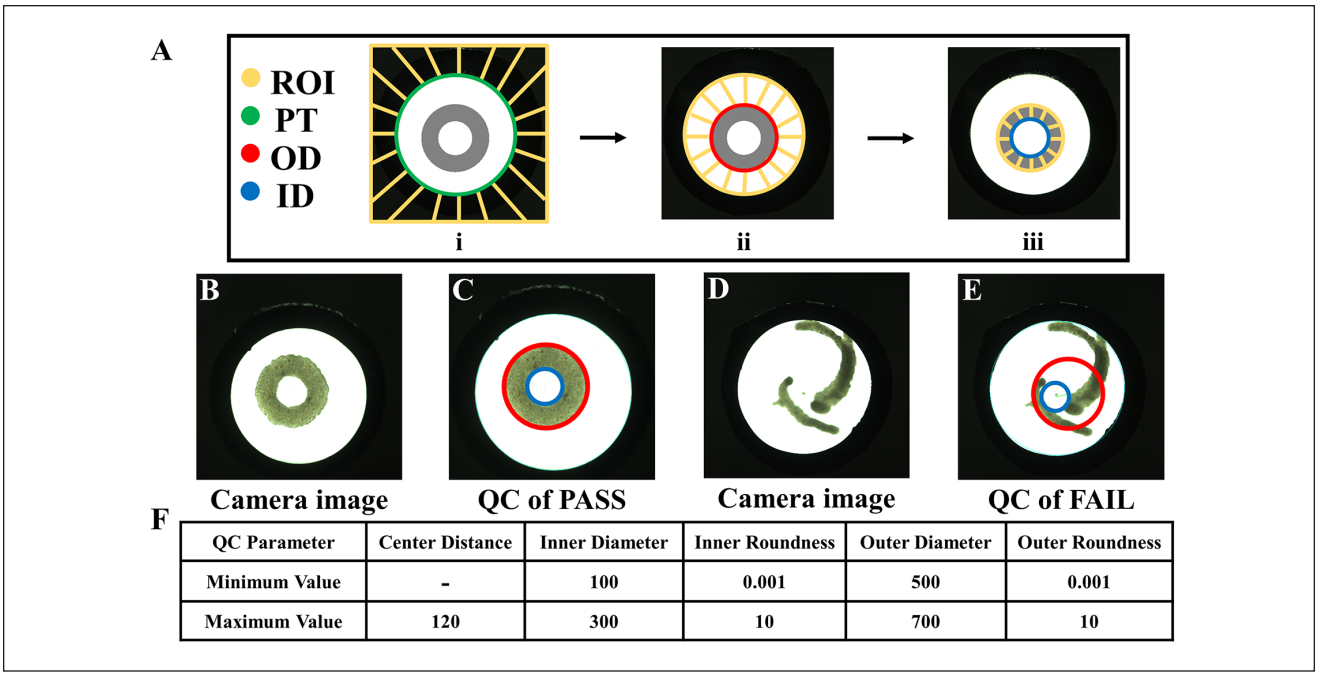

F

QC Parameter	Center Distance	Inner Diameter	Inner Roundness	Outer Diameter	Outer Roundness
Minimum Value	-	100	0.001	500	0.001
Maximum Value	120	300	10	700	10

Figure 6. Image-based quality control (QC) of tissue rings. A custom algorithm for QC was developed to locate the outer diameter (red circle) and inner diameter (blue circle) of a tissue ring inside the pipette tip (**A**), measure given parameters, compare these values to set values, and determine if the ring passes or fails. The algorithm uses an ROI (yellow) to identify the pipette tip (green) (i), the outer diameter of the tissue ring (red) (ii), and the inner diameter of tissue ring (blue) (iii). Images of a human umbilical vein endothelial cell (HUVEC) ring (1.5×10^5 cells) (**B**, **C**) and a malformed ring (**D**, **E**) inside the pipette tip were processed using the algorithm. Output of an acceptable ring that passes QC and would be deposited into the funnel-guide (**C**), where the red circle shows the QC-identified outer diameter and the blue circle shows the QC-identified inner diameter. Output of an unacceptable malformed ring that fails QC and would be discarded back into the well plate (**D**), where the red circle shows the QC-identified outer diameter and the blue circle shows the QC-identified inner diameter. Tabulated QC parameters and the acceptable value ranges for HUVEC rings (**F**).

validate luminal alignment of the tissue rings, a dissecting microscope was used to take a top-down image of the bio-tube while inside the stacking chamber. Light was clearly visible through the center of the lumens, showing ring alignment.

Discussion

Since its inception nearly 40 y ago, tissue engineering has been largely confined to academic research institutions, and because of numerous challenges as well as a gap in manufacturing technologies, there has been limited success in commercial settings. To help address this issue, more work is needed to develop new automated manufacturing processes for tissue-related technologies.[1] Here, we describe the automation of the funnel-guide, an additive manufacturing method that uses tissue rings as building units to form bio-tubes.[26] All automated manufacturing processes require suitable building materials and a fundamental understanding of their inherent properties. The use of living cells in tissue engineering presents new and exciting challenges to both automation and manufacturing. Significant advances in laboratory automation have set the stage for developing new manufacturing strategies for the emerging field and industry of 3D tissue engineering. In this article, we address several of those challenges in the context of using a liquid-handling robot to automate the funnel-guide. The fundamental building unit of these bio-tubes is a ring-shaped microtissue comprised of tens of thousands of cells. We show that these building units can be produced via an easily automated process and, more importantly, that these units can be used to build bio-tubes layer by layer via automation of the funnel-guide.

To facilitate the automated production of ring-shaped building units, we designed a new micromolding system for standard 96-well plates used in laboratory automation. Each well contains a single ring-shaped recess molded in agarose. Because agarose is nonadhesive for cells, cells pipetted into the well settled into the recess, aggregated, and self-assembled around a central conical peg (1.1 mm tall) of agarose to form a ring-shaped microtissue, one per well, in less than 20 h. The resulting ring-shaped building units have an outer diameter of about 1.77 mm, an inner diameter of about 1.2 mm, a z thickness of about 275 µm, a volume of about 5.8×10^8 µm^3, and are comprised of between 100,000 to 200,000 living cells. The processes by which cells aggregate and self-assemble is very complex and

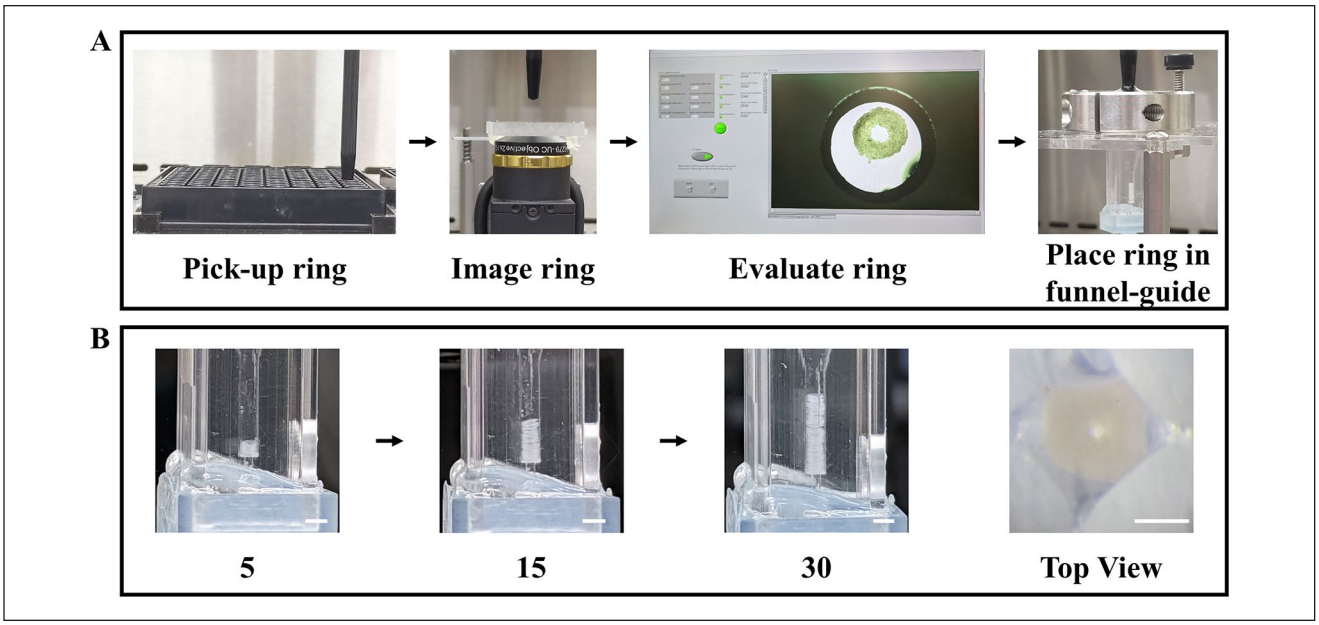

Figure 7. Automated fabrication of bio-tubes. Images of the key steps of the automated fabrication process (**A**). A single tissue ring is picked up from the well of a 96-well plate by liquid suction and imaged while suspended at the air-liquid interface using an upward-facing camera. The captured image is used to perform real-time quality control via a custom LabVIEW interface. If the tissue ring falls within the range of the specified quality control parameters, it is then delivered to the funnel-guide. Images of bio-tube fabrication (**B**). Bio-tubes are constructed via the addition of individual tissue rings, which are guided into the stacking chamber via the funnel chamber of the funnel-guide. As more tissue rings are added, the stack grows in height. Alignment of the tissue rings is shown via a top-down image of the final stack of 30 rings inside the stacking chamber, where light from the bottom of the stack can be seen through the lumens. Scale bars are 2 mm, 2 mm, 2 mm, and 1 mm, respectively.

involves numerous cellular processes that include, but are not limited to, cell-cell adhesions, cytoskeletal contraction, cell migration/deformation, and synthesis of extracellular matrix proteins. These dynamic processes cause these living rings to undergo morphological changes that can alter their size and shape, thus presenting new challenges to the manufacture of uniform building units. Moreover, although nearly all cell types perform these complex cellular activities, there are significant differences between cell types that can further affect the fabrication of building units.

As the rings contracted around the cone, they climbed upward. The cone shape and upward motion of the rings helped facilitate their removal from the well by the fluid suction of a pipette, which is a key aspect of our automated workflow. The formation of rings as well as retrieval of rings in ANSI/SLAS 96-well plates offer numerous advantages in laboratory automation including the use of liquid-handling robots to scale up the production and retrieval of tissue rings as well as the use of existing robotic workflows and integrated equipment for cell culture, imaging, and biochemical assessments. If larger rings are needed, a similar strategy can be adapted to 48- or 24-well plates to produce rings with inner diameters of about 2.5 mm and 5 mm, respectively. So long as the ring can fit inside a wide-bore pipette tip, the retrieval can be automated using a liquid-handling robot.

The successful formation of rings and their rate of upward movement varied with cell type and was influenced by the angle of the agarose cone as well as the number of cells seeded. Both HepG2s and HUVECs required a minimum number of cells to successfully form rings. HepG2 rings climbed more slowly up the cone and were more influenced by the cone's angle than HUVEC rings. These data are consistent with a previous study that demonstrated cell-type differences in the rate of ring movement up a cone.[27]

As the rings moved up the cone, they underwent morphological changes, most notably a decrease in the diameter of their lumen. As a building unit, the lumen diameter is an important feature because it dictates the size of the lumen of the bio-tube to be built. Because the ring contacts with and contracts around the cone, the diameter of the ring's lumen is dictated by the cone's shape and the ring's height on the cone, or how high the ring has moved. As with ring formation, this motion is dependent on time, cell type, number of cells seeded, and cone geometry. Seeding a well with a specified number of cells and harvesting the resulting ring at a specific time yields a building unit of defined size and shape. However, as our data also demonstrate, mold design and time of harvest are not sufficient; cell type must also be factored in when designing the process for making building units. HepG2 and HUVEC rings varied in their number of cells needed to form rings as well as the rate of ring movement up the cone.

Morphological changes to the ring building unit continued after the ring was harvested from the cone. Both HepG2 and HUVEC rings contracted and slowly decreased the diameter of their lumens over time, but this process was significantly slower (hours) than the rate of contraction while on the peg and provided more than sufficient time (minutes) to retrieve a ring building unit and transfer it to the funnel-guide before the occurrence of a significant morphological change. Interestingly contraction of HepG2 rings was significantly slower than HUVEC rings, further demonstrating cell type–specific differences.

Together, these data demonstrate that the ring building unit is a dynamic 3D structure that undergoes significant changes as it is formed by tens of thousands of living cells. We have shown that it is possible to direct and harness these changes, thereby rendering them predictable and making it possible to produce ring-shaped building units of defined size and shape. The major factors are the mold design (diameter of circular recess and the shape/angle of the central conical peg), the number of cells seeded, and the time at which the ring is retrieved from the peg. There are differences between cell types, but these differences are easily controlled by adjusting the shape/angle of the central conical peg, the number of cells seeded, and/or the time at which the ring is retrieved from the peg. Future studies will continue to evaluate the differences between rings formed from various cell types and combinations of cell types. This information will inform the construction of bio-tubes for organ systems containing multiple relevant cell types, such as a blood vessel composed of endothelial cells and smooth muscle cells. We could also investigate methods of stabilizing the contractile building parts using physical and biological inhibitors.[27,28] For example, once stacked, the bio-tube could be perfused to apply radial pressure to stagnate continued morphological changes.[29,30]

The ability to retrieve a ring one at a time enabled us to devise a QC step based on visual inspection. When a ring was retrieved, we observed that the ring quickly settled to the liquid-air interface at the bottom of the pipette tip and could be visualized by an upward-facing camera. Acceptable images required optimal lighting as well as careful adjustment of the convex liquid surface, which created a lens effect that could distort the image. Ring intactness as well as the inner and outer diameter of the ring could be quickly identified to determine if a building part was suitable for transfer to the funnel-guide. The ability to quickly inspect building parts before use is an important addition to a robust automated manufacturing process, especially additive manufacturing. If a single defective ring were incorporated into the build of a bio-tube, it would ruin the entire build. In addition to simple morphologic criteria, other optical parameters as well as other imaging modalities could be used to assess in real time the suitability of a ring building unit.

Once a ring was deemed suitable, it was transferred by the liquid-handling robot to the funnel-guide, where simple contact between the pipette tip and the surface of the liquid in the funnel-guide released each ring. Within a maximum of 43 s, each ring had slowly settled in the funnel-guide by gravity to land on a stack of rings that fused into a bio-tube. The automated work flow for building bio-tubes had three major steps: (1) ring pick up, (2) ring imaging/evaluation, and (3) ring deposit in the funnel-guide. The cycle time between the addition of two rings to the funnel-guide was 28 s, and it took approximately 45 min to build a bio-tube containing 96 rings. Individual ring building units have a z height of about 275 μm, so all rings from a single 96-well plate could produce a stack of rings with a starting height of about 2.64 cm. Each ring is about 100,000 to 200,000 thousand cells compared to about 1000 cells in a single spheroid, which is another building unit used in additive manufacturing. Thus, compared with spheroid building units, ring building units decrease the number of manufacturing steps by a factor of about 100.

In this study, we demonstrated a proof-of-concept that we can automate funnel-guided bio-tube fabrication using a modified off-the-shelf liquid-handling robot. This provides an advantage over existing systems, such as the Kenzan and robotic assembly of vascular tissue, in which the spheroid and ring tissue parts are removed from the culture medium during the build process.[18,21] In addition, our method does not require the tissue to be punctured with needles or strung through a mandrel for alignment, decreasing tissue part manipulation. Future experiments will include the development of a perfusion system connected to the base of the funnel-guide to ensure appropriate distribution of nutrients and continued improvements to the QC algorithm. Future iterations of the algorithm could incorporate an object-counting function, which would exclude images with excess cellular debris, and could incorporate elliptical best-fit features to better approximate the variety of luminal shapes.

In summary, we have modified a standard liquid-handling robot and ANSI/SLAS 96-well plates to develop an automated process for additive manufacturing of bio-tubes from ring-shaped building units. We provide the means and fundamental knowledge to scale up the production of ring-shaped building units of prescribed size and shape that are composed of more than 100,000 living cells. Our automated process includes the retrieval of rings one at a time from a 96-well plate and a new QC step in which rings are visually inspected in real time before they are transferred to the funnel-guide for bio-tube formation. This work helps demonstrate that laboratory automation can help solve the manufacturing bottleneck in the field of tissue engineering.

Acknowledgments

The authors would like to thank Joshua Manning for his assistance in capturing photographs and videos and Blanche C. Ip, PhD, and Benjamin Wilks for their assistance with statistical analysis.

Declaration of Conflicting Interests

The authors declared the following potential conflicts of interest with respect to the research, authorship, and/or publication of this article: Jeffery R. Morgan has an equity interest in Microtissues, Inc. This relationship has been reviewed and is managed by Brown University in accordance with its conflict of interest policies.

Funding

The authors disclosed receipt of the following financial support for the research, authorship, and/or publication of this article: This work was funded by a grant from the National Science Foundation NSF PFI-TT-3 12554728.

ORCID iD

Kali L. Manning https://orcid.org/0000-0003-4488-0188

References

1. Advanced Regenerative Manufacturing Institute. https://www.armiusa.org/ (accessed Nov. 26, 2019).
2. Thomas, R. J.; Chandra, A.; Liu, Y.; et al. Manufacture of a Human Mesenchymal Stem Cell Population Using an Automated Cell Culture Platform. *Cytotechnology* **2007**, *55*, 31–39.
3. Marga, F.; Jakab, K.; Khatiwala, C.; et al. Toward Engineering Functional Organ Modules by Additive Manufacturing. *Biofabrication* **2012**, *4*, 022001.
4. Norotte, C.; Marga, F. S.; Niklason, L. E.; et al. Scaffold-Free Vascular Tissue Engineering Using Bioprinting. *Biomaterials*. **2009**, *30*, 5910–5917.
5. Murphy, S. V; Atala, A. 3D Bioprinting of Tissues and Organs. *Nat. Biotechnol*. **2014**, *32*, 773–785.
6. Li, Y.; Zhang, T.; Pang, Y.; et al. 3D Bioprinting of Hepatoma Cells and Application with Microfluidics for Pharmacodynamic Test of Metuzumab. *Biofabrication* **2019**, *11*, 034102.
7. Swaminathan, S.; Hamid, Q.; Sun, W.; et al. Bioprinting of 3D Breast Epithelial Spheroids for Human Cancer Models. *Biofabrication* **2019**, *11*, 25003.
8. Faramarzi, N.; Yazdi, I. K.; Nabavinia, M.; et al. Patient-Specific Bioinks for 3D Bioprinting of Tissue Engineering Scaffolds. *Adv. Healthc. Mater*. **2018**, *7*, e1701347.
9. Ashammakhi, N.; Hasan, A.; Kaarela, O.; et al. Advancing Frontiers in Bone Bioprinting. *Adv. Healthc. Mater*. **2019**, *8*, 1801048.
10. Mekhileri, N. V.; Lim, K. S.; Brown, G. C. J.; et al. Automated 3D Bioassembly of Micro-Tissues for Biofabrication of Hybrid Tissue Engineered Constructs. *Biofabrication* **2018**, *10*, 024103.
11. Rago, A. P.; Dean, D. M.; Morgan, J. R. Controlling Cell Position in Complex Heterotypic 3D Microtissues by Tissue Fusion. *Biotechnol. Bioeng*. **2008**, *102*, 1231–1241.
12. Napolitano, A.; Dean, D.; Man, A.; et al. Scaffold-Free Three-Dimensional Cell Culture Utilizing Micromolded Nonadhesive Hydrogels. *Biotechniques*. **2007**, *43*, 494–500.
13. Livoti, C. M.; Morgan, J. R. Self-Assembly and Tissue Fusion of Toroid-Minimal Building Units. *Tissue Eng. Part A*. **2010**, *16*, 2051–2061.
14. Strobel, H. A.; Hookway, T. A.; Piola, M.; et al. Assembly of Tissue Engineered Blood Vessels with Spatially-Controlled Heterogeneities. **2018**, *508*, 1–42.
15. Fleming, P. A.; Argraves, W. S.; Gentile, C.; et al. Fusion of Uniluminal Vascular Spheroids: A Model for Assembly of Blood Vessels. *Dev. Dyn*. **2010**, *239*, 398–406.
16. Leary, E.; Rhee, C.; Wilks, B. T.; et al. Quantitative Live-Cell Confocal Imaging of 3D Spheroids in a High-Throughput Format. *SLAS Technol*. **2018**, *23*, 231–242.
17. Kelm, J. M.; Djonov, V.; Ittner, L. M.; et al. Design of Custom-Shaped Vascularized Tissues Using Microtissue Spheroids as Minimal Building Units. *Tissue Eng*. **2006**, *12*, 2151–2160.
18. Nycz, C. J.; Strobel, H. A.; Suqui, K.; et al. Method for High-Throughput Robotic Assembly of Three-Dimensional Vascular Tissue. *Tissue Eng. Part A*. **2019**, *25*, 1251–1260.
19. Moldovan, N. I.; Hibino, N.; Nakayama, K. Principles of the Kenzan Method for Robotic Cell Spheroid-Based Three-Dimensional Bioprinting. *Tissue Eng. Part B. Rev*. **2017**, *23*, 237–244.
20. Itoh, M.; Nakayama, K.; Noguchi, R.; et al. Scaffold-Free Tubular Tissues Created by a Bio-3D Printer Undergo Remodeling and Endothelialization When Implanted in Rat Aortae. *PLoS One*. **2015**, *10*, e0145971.
21. Machino, R.; Matsumoto, K.; Taniguchi, D.; et al. Replacement of Rat Tracheas by Layered, Trachea-Like, Scaffold-Free Structures of Human Cells Using a Bio-3D Printing System. *Adv. Healthc. Mater*. **2019**, 1800983.
22. Arai, K.; Murata, D.; Verissimo, A. R.; et al. Fabrication of Scaffold-Free Tubular Cardiac Constructs Using a Bio-3D Printer. *PLoS One*. **2018**, *13*, e0209162.
23. Ip, B. C.; Cui, F.; Wilks, B. T.; et al. Perfused Organ Cell-Dense Macrotissues Assembled from Prefabricated Living Microtissues. *Adv. Biosyst*. **2018**, *2*, 1800076.
24. Blakely, A. M.; Manning, K. L.; Tripathi, A.; et al. Bio-Pick, Place, and Perfuse: A New Instrument for Three-Dimensional Tissue Engineering. *Tissue Eng. Part C Methods* **2015**, *21*, 737–746.
25. Ip, B. C.; Cui, F.; Tripathi, A.; et al. The Bio-Gripper: A Fluid-Driven Micro-Manipulator of Living Tissue Constructs for Additive Bio-Manufacturing. *Biofabrication* **2016**, *8*, 025015.
26. Manning, K. L.; Thomson, A. H.; Morgan, J. R. Funnel-Guided Positioning of Multicellular Microtissues to Build Macrotissues. *Tissue Eng. Part C Methods* **2018**, *24*, 557–565.
27. Youssef, J.; Nurse, A. K.; Freund, L. B.; et al. Quantification of the Forces Driving Self-Assembly of Three-Dimensional Microtissues. *Proc. Natl. Acad. Sci. U.S.A*. **2011**, *108*, 6993–6998.
28. Susienka, M. J.; Wilks, B. T.; Morgan, J. R. Quantifying the Kinetics and Morphological Changes of the Fusion of Spheroid Building Blocks. *Biofabrication* **2017**, *8*, 045003.
29. Moya, M. L.; Hsu, Y.-H.; Lee, A. P.; et al. In Vitro Perfused Human Capillary Networks. *Tissue Eng. Part C Methods* **2013**, *19*, 730–737.
30. Phan, D. T. T.; Wang, X.; Craver, B. M.; et al. A Vascularized and Perfused Organ-on-a-Chip Platform for Large-Scale Drug Screening Applications. *Lab Chip* **2017**, *17*, 511–520.